Matonti C, Attree N, Groussin O, Jorda L, Viseur S, Hviid SF, Bouley S, Nébouy D, Auger A, Lamy PL, Sierks H, Naletto G, Rodrigo R, Koschny D & Davidsson B (2019) Bilobate comet morphology and internal structure controlled by shear deformation. *Nature Geoscience*, 12, pp. 157-162. https://doi.org/10.1038/s41561-019-0307-9

Supplementary information for

Internal structure of bilobate comets revealed by erosion from shear deformation

This PDF file includes:

Supplementary Information
Supplementary Discussion
Supplementary Figures. 1 to 10
References (46) to (53)

Table of contents

Supplementary Information
Image descriptions and pattern interpretations

1. Geb and Atum regions

1.1

In the Geb region, the image NAC_2014-09-30T08.54.41.560Z_ID30_1397549700_F22 shows brittle material in a ≈ 500 m wide zone (Supplementary Fig. 3a). In addition to the pervasive isotropic fractures (in blue in Supplementary Fig. 3) forming meter-scale polygonal network (e.g.[11],[12]). Two other types of lineaments, showing crosscutting relationships are observed. (i) First, straight, oblique 10 - 100 m lineaments (in green in Supplementary Fig. 3), which are cut by the second type of lineaments. (ii) Second, hectometres long lineaments (in red in Supplementary Fig. 3b, which are analogue to type-2 lineament in Fig. 1) which crosscut all the others, and show branching extremities (left arrow in Supplementary Fig. 3b), anastomosing structures delimiting lenticular-shaped blocks, and bending extremities at relay zones (right arrow in Supplementary Fig. 3b). This implies mechanical interaction between these lineaments during their formation, that could not exist for instance in the case of primordial layer lineaments.

The fact that one type of lineament cuts another one necessarily implies (following the crosscutting relationship principle[15]) that it postdates it. Therefore, such a lineament cannot be a primordial feature (such as a layer) but is a structural feature (such as fractures or faults), as the type-2 lineaments are. Moreover, the polygonal lineaments have been clearly assessed as fractures, confirming that type 2 lineaments must be fractures too.

Such an array of fractures, showing bends, interconnections and branching structures on the longest ones is strikingly similar to structures found on Earth (Supplementary Fig. 3 blue insert), which can be found in a context of strike-slip/shear faulting, known as “synthetic branching fault structures” (Fig. 1b3 and d3 and Supplementary Fig. 3d, e.g.[17,46]).

Moreover, at the intersection between the longest type-2 fractures (in red in Supplementary Fig. 3c) and type-1 straight lineaments (in green in Supplementary Fig. 3c) meter-scale offsets are likely present. These offsets are all of the same direction and are consistent over the entire length of the lineaments (red arrows in Supplementary Fig. 3c). This strongly suggests that the longest (type-2) fractures have been affected by a slip motion along their plane at some point in their history, and perhaps are actually fault-like objects characterised by a sinistral strike-slip-motion, typical of a shear deformation context (double arrow in Supplementary Fig. 3c).

1.2

In the Geb/Atum regions, the image NAC_2014-10-06T01.15.53.548Z_ID10_1397549100_F22 shows mainly brittle material, outcropping over an area of ≈ 600 m (Supplementary Fig. 4). Two types of lineaments are present: (i) again the pervasive, meter-scale polygonal fractures (in blue in Supplementary Fig. 4). (ii) Parallel hectometres long lineaments that are partially overlapping, following a right-stepping *en-échelon* structure[17], between which oblique subsidiary decameter fractures exist (in red in Supplementary Fig.4b, analogue to the type-2 lineaments from the previous sections).

An elongated hectometre long and decametre deep (≤20 m) central depression occurs between the longest fractures. Oblique fractures are present in this depression, delimitating blocks that form metre-to-decametre-high topography on the central depression floor (red dashed box in Supplementary Fig. 4a). These blocks fit with the shape of the scarps observed in the depression's left border (white arrows in Supplementary Fig. 4d) and thus seem to have been broken-down/eroded and lowered from the side' cliff/walls of the depression.

The extremity of the leftmost fracture shows curved branching sub-fractures, which all merge with the longest fracture at the same point (arrow in Supplementary Fig. 4b). This kind of pattern is again very similar to a typical fault termination known as a splay or "imbricated fan"[17], which exist in "transpressive" contexts, and suggests that the long *en-échelon* lineaments

are a set of faults formed in a shear context. This would also explain the occurrence of the central depression that might originate from a pull-apart-like extensional structure, typically formed between shear strike-slip faults and inducing block rotations[47] (arrows on Supplementary Fig. 4d).

2. Southern hemisphere and equator: Neck borders and central Neck areas.

2.1

Images NAC_2016-01-28T05.33.00.986Z_ID30_1397549000_F22 and NAC_2016-01-27T18.20.08.974Z_ID30_1397549000_F22 both show mainly brittle material with scattered small dust covered zones, over the entire Southern hemisphere of 67/P (>2.5 km, Fig. 1 and Supplementary Fig. 5). On the borders of the neck, especially in the Wosret region, 2 types of lineaments are observed. The highly self-parallel lineaments (type-1 lineaments), which are compatible with layers as interpreted in previous studies (e.g. [3,9,13]), and a network of fractures (Type 2 lineaments) composed of decametre-to-hectometre scale fractures (max length is 450 m) that crosscut the layers (Fig. 1d1-2, Supplementary Figs. 5b and 5d). On the small-lobe side of the neck (leftmost part) of the images NAC_2016-01-28T05.33.00.986Z_ID30_1397549000_F22 (Supplementary Figs. 5a-b, especially in the lower-left corner of the image), NAC_2016-01-27T19.28.00.047Z_ID30_1397549800_F22 (Supplementary Figs. 5c-d) and NAC_2016-01-27T18.20.08.974Z_ID30_1397549000_F22 (Supplementary Fig. 6a), layer lineaments are clearly following the topography contour lines, and hence cut the surface of 67P at low angles, forming terraces and plateaus. This indicates they are sub-parallel to the nucleus surface in this area. Layers dip-angle to the surface of the nucleus is even more visible in the Hathor equatorial region, where layers type-1 lineaments clearly follow the topography contour line (see Supplementary Fig. 7 c-d).

2.2

On the neck borders, the longest (>100 m) fractures are formed of 2 sets, oriented along 2 main directions, forming a 30 to 40° angle. They are arranged in an anastomosing pattern, composed of highly interconnected fracture, bending one toward another, that delimit lenticular hectometres long and decametres wide blocks oriented preferentially parallel to the neck axis/direction (Fig. 1 and Supplementary Fig. 5). Such a fracture pattern indicates mechanical interaction during the fracturing process, suggesting they all formed together and by the same process. Moreover, the currently observed highly inter-connected anastomosing patterns need progressive and continuous deformation to form (e.g. typically tens of thousands to millions of years on Earth) and cannot be the result of a brutal, almost instantaneous, impact event, despite the fact that an initial impact during lobe-merger could have weakened the nucleus material in the future neck area. This pattern is also very consistent with typical strike-slip fault-zone or shear-zones deformation contexts (e.g. [19,20,46,48], Figs. 1b3 and 1d3). Limited inside the rightmost lenticular block (Fig. 1d1-2), a dense set of oblique decametre-scale fractures occurs (red arrow in Fig 1d1-2 and Supplementary Fig. 5a-b). Such a block/lens structures also point to shear deformation as the fracturing process here, being a typical structure that forms in material sheared between two bounding discontinuities or faults (Fig 1e3)[21,49].

These fracture lineaments, which are the intersection of 3D fractures planes with the topographic surface, show no bend/deviation where they encounter topographic slopes, indicating they cut 67P's surface at high angle, i.e.t they are sub-vertical.

2.3

In the central part of the neck (Neith, Sobek and Anhur regions), the nucleus shows a rougher surface. In this zone, layer lineaments become less continuous and little-to-not visible (in green in Supplementary Fig. 5b). We observe decametre wide lenticular shaped ridges of brittle material which are affected by oblique fractures (Fig. 1e1), alternating with zones of chaotic

material displaying no visible structure (in grey Fig. 1e2). These ridges are similar to the structure observed in the neck border (Fig 1d2), and arranged *en-échelon*, along one of the 2 main fractures directions found in Wosret (Fig. 1c). As in the neck border, such a kind of structure can be related to the occurrence of sheared blocks, pinched between 2 minor strike-slip faults and showing typical shear fractures (e.g. [21,49,50]) oblique to the bounding fault directions (Fig. 1e2). The chaotic zones around these sheared lenses are compatible with the maximum deformation zone, usually located at the centre of a sheared zone[22] and characterised by crushed material showing no large scale structure (Supplementary Fig. 6b). This is compatible here with the unstructured/chaotic zones, which we assume are formed of crushed material composed of blocks of decameter to <1 m size (Fig. 1e1 and supplementary Fig. 6).

We don't observe polygonal fracture networks around the neck centre, suggesting a still-active mechanical erosion process that currently renews the nucleus surface, impeding polygonal fractures development and preservation in this zone. Far from the neck (>1 km), fracture directions become more scattered and isotropic (Supplementary Fig. 6a), their lengths drop to the meter scale, being more likely associated with background thermal fractures.

2.4

Image NAC_2014-09-22T08.52.08.332Z_ID30_1397549001_F41 shows the Hapi/Hathor NH equatorial area. It shows a mount-like topography with a vertical cliff face, relative to the local gravity vector (Supplementary Fig. 7a). In this zone, we were able to study and trace the fracture lineaments along their horizontal direction (at Bakhu's top, Supplementary Fig. 7c-d) and vertical direction (toward depth, Supplementary Fig. 7a-b) along the Bakhu cliff. The zone is characterised by a network composed of 2 sets of fractures, observed along their vertical direction, and presenting 2 opposite dip angles (of about 60-80°) (Supplementary Fig. 7b).

Toward the centre of the neck, altitude decrease and we observe a dense set of fractures, which is compatible with increasing deformation level, and can be observed in faulted or

sheared-zone contexts (Supplementary Fig. 7b). Such 3D analyses, following individual fractures along their strike (horizontal) and dip (vertical) have also been possible at the transition between the Sobek and Hapi/Bastet regions.

We found no clear crosscutting relationship between these fractures, suggesting they formed concomitantly, with a similar process. These fractures have also been observed in top-view (NAC_2016-06-16T09.32.11.500Z_ID30_1397549300_F22, Supplementary Fig. 7c-d) where they show the same 2 preferential directions found in the SH neck border regions (Fig1 and Supplementary Fig.5). They exhibit also the same clear, diamond-shaped fracture pattern, characteristic of the Riedel-shear structure (Supplementary Fig. 7d). Riedel shear structures are a classical pattern of fractures found in a material affected by shear deformation. They are characterized by 5 types of plane, forming characteristic angles which depend on the mechanical properties of the material. Depending on the grade of the deformation, the stress, and the physical properties of the material, two or more of these planes exist in the material[26,27,28]. R' Riedel shear fractures are known to be less visible/developed than P and R. In 67P case, the direction of the 2 principal directions of the fractures match with the occurrence of P and R shear fractures; Y shear represented by the overall shear structure direction (e.g. the dense fractures near the centre of the neck and the direction of the sheared lenses/ridges).

3. Northern hemisphere: Neck borders

In the NH neck regions, although less visible due to dust cover, long fractures (>30m) also exhibit two principal directions and the same Riedel-shear pattern (Supplementary Figs 7 and 9). It is observable in the equatorial mount region (Bakhu, Supplementary Fig. 7) and in the centre of Hapi (Supplementary Fig. 9a).

Supplementary Discussion

Reasons for 67P to exhibit highly Earth-similar deformation structures

Considering that shear deformation/faulting is mainly caused on earth by geodynamic processes that likely cannot exist on 67P, what can be the causes of these deformations? The occurrence of very Earth-like structures at the surface of a comet nucleus, which is characterised by extremely low gravity force[29] (1/10000 Earth's) and low material strength, (few Pa to hundreds of Pa, [30,33,34]) is rather unexpected. However, considering that similar gravity stress to material strength ratios exist on 67P and Earth (35-170×10^3 VS. 51×10^3 respectively[29]), we can argue that mechanical parameters scale well between 67P and Earth. Therefore, mechanically analogous conditions should exist on these 2 bodies, as observed for instance in laboratory experiments of meter-scale lithosphere analogue models (e.g. [51]). Besides, although 67P's nucleus seems to have very low bulk mechanical strength, nucleus material clearly exhibits fracture, hence a brittle behaviour. This is because the brittleness characteristic of a material is more linked to the ratio of tensile strength to compression strength[52] rather than the magnitude of these moduli.

Supplementary Figures and Captions:

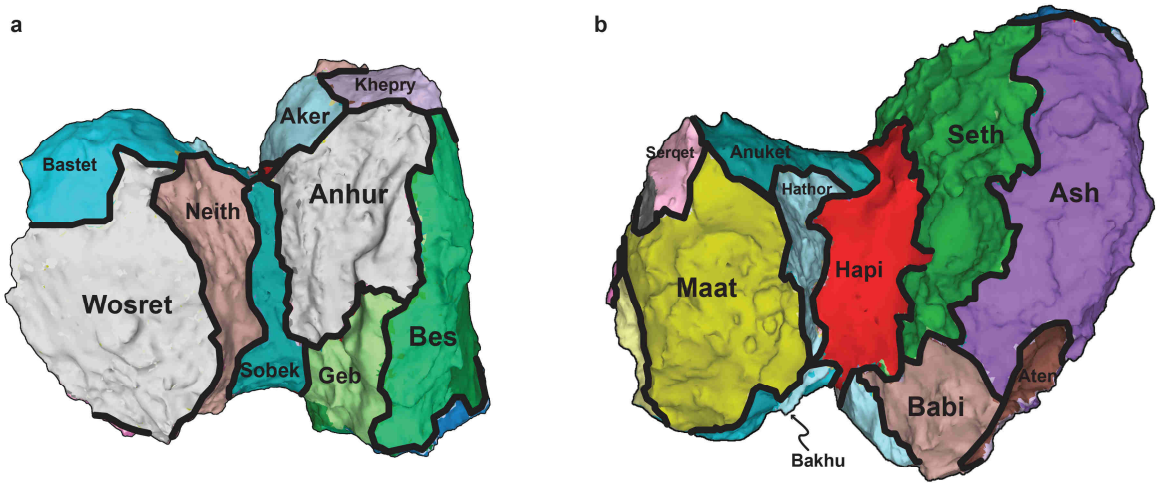

Supplementary Figure 1: Regions of 67P mapped on the 3D shape model. a. View of the southern hemisphere regions; b. View of the northern hemisphere regions, showing the newly named Bakhu mount area.

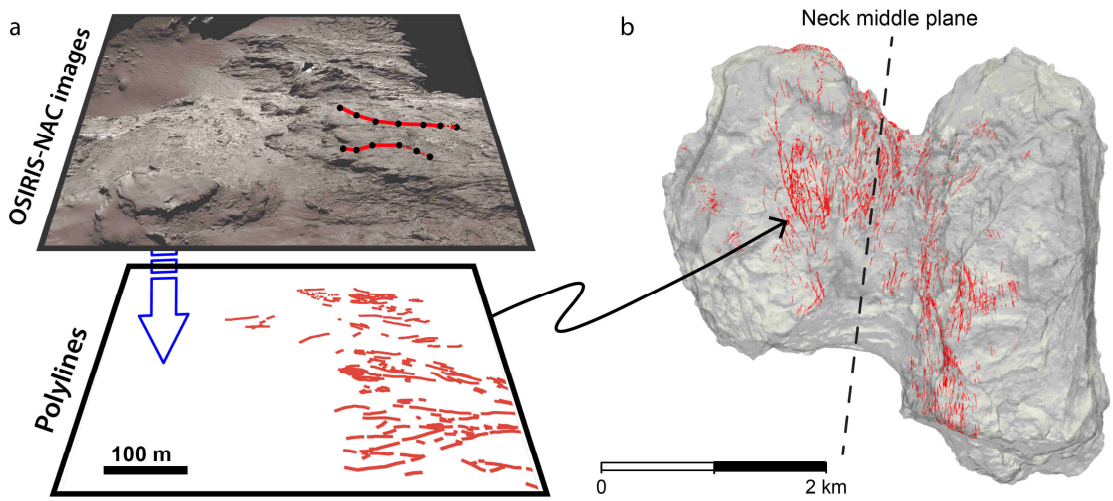

Supplementary Figure 2: Methodology used for fracture lineament analyses. a. Example of OSIRIS-NAC image with digitalised fracture lineaments as polylines (in red). b. Screen capture of 67P shape model (cg-dlr_spg-shap7-v1.0) facing the southern Hemisphere, showing (in red) a part of the projected fractures. Dashed line represents the Neck middle plane constructed from[25].

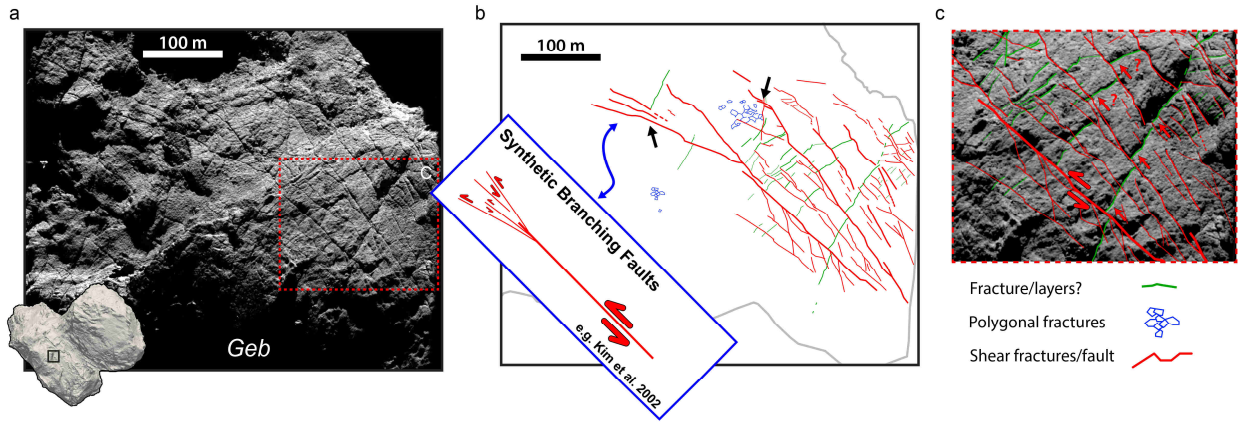

Supplementary Figure 3: Fracture patterns and their interpretation in the Geb region. a. Crop of NAC_2014-09-30T08.54.41.560Z_ID30_1397549700_F22 image of brittle material showing pervasive fractures networks. b. Digitalised pattern showing the 3 different lineaments (polygonal fractures in blue, type 1 in green and type 2 in red). Type 2 is characterised by bending (right black arrow) and branching termination (left arrow), that can be related to a shear context. Blue insert showing similarity with a typical fault branching termination. c. Zoom on the image showing possible offsets of type 1 lineaments (likely layers) by the type 2 lineaments (fractures) which strongly suggests the existence of strike-slip fault-like structures, also compatible with shear deformations.

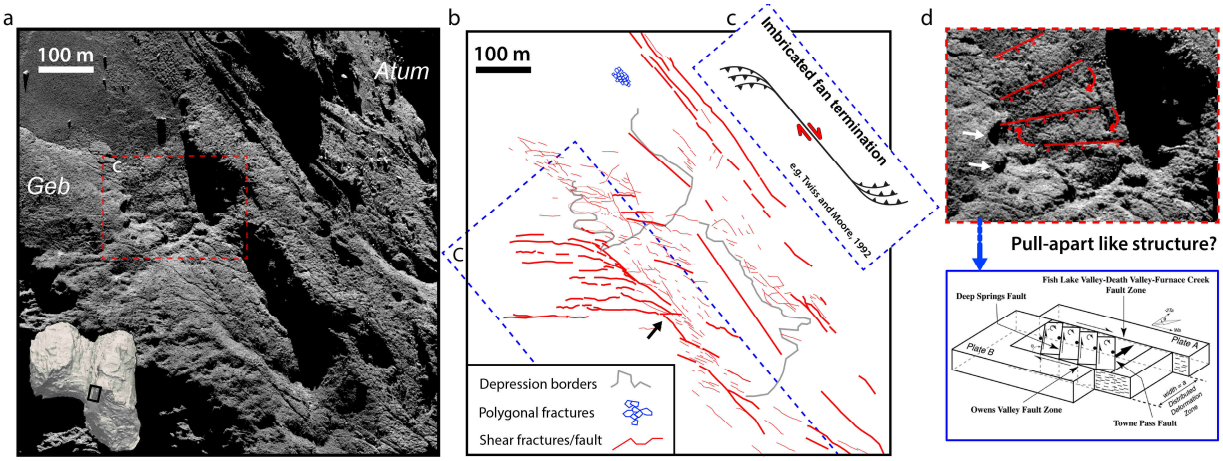

Supplementary Figure 4: Fracture pattern and morphology in the Geb/Atum region. a. NAC_2014-10-06T01.15.53.548Z_ID30_1397549100_F22 image of brittle material showing hectometre fractures delimiting a central elongated depression. b. Digitalised fracture pattern, showing fault-like termination along with right stepping *en-échelon* arrangement that matches with the occurrence of a shear-fault cluster. c. Scheme of typical imbricated-fan fault termination, similar to what is observed in the image (blue dashed-box on b). d. Zoom on rotated and lowered blocks accounting for possible pull-apart basin structure (blue insert: classical pull-apart structure from[47]).

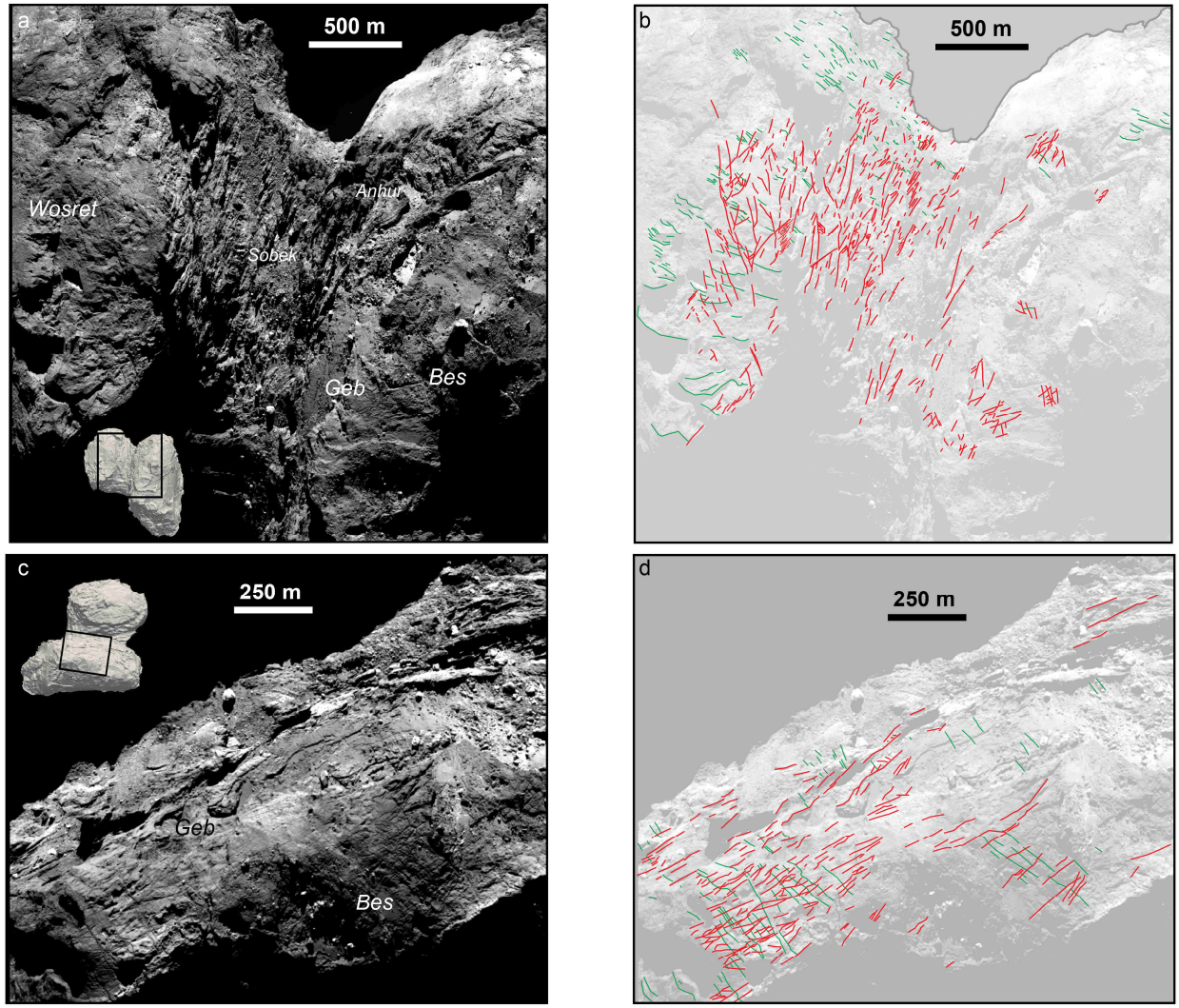

Supplementary Figure 5: 67P global southern hemisphere fracture and layer pattern. a. NAC_2016-01-28T05.33.00.986Z_ID30_1397549000_F22 image showing the neck and surrounding lobe regions in the SH. b. Digitalised possible layers (in green) forming terraces on the lower-left part of the image, indicating that they are sub-horizontal to the topography. Fractures (in red) showing 2 main directions, on average sub-parallel to the neck midplane. c. Crop of NAC_2016-01-27T19.28.00.047Z_ID30_1397549800_F22 image showing Anhur big lobe region. d. Digitalised lineaments characterised by parallel, non-crosscutting and sub horizontal possible layers (in green), crosscut by sub-vertical interconnected fractures (in red).

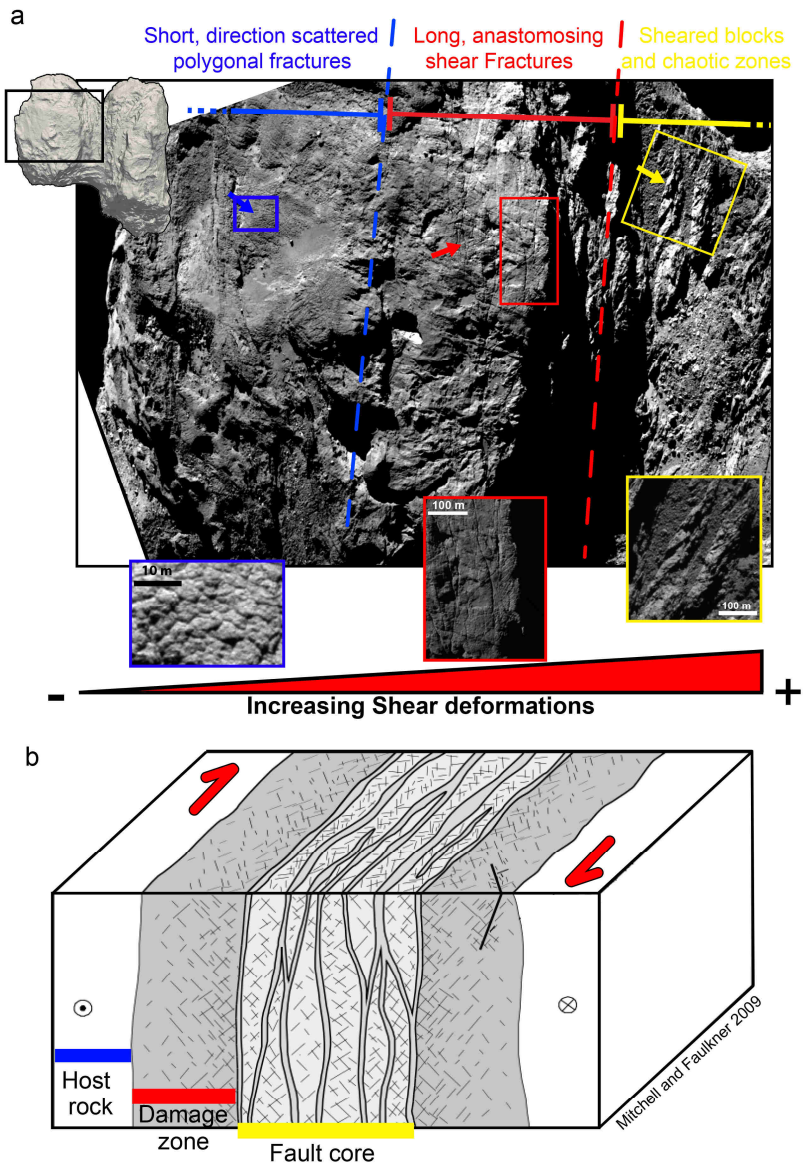

Supplementary Figure 6: Evolution of fracture pattern and deformation features on the small lobe associated with increasing shear deformation, relative to the neck centre distance. a. NAC_2016-01-27T18.20.08.974Z_ID30_1397549000_F22 image showing a contrasting fracture pattern toward the neck centre. It is dominated far from the neck by the background meter-scale isotropic polygonal fractures, on the neck border by hectometre-scale (mainly neck parallel), branching and anastomosing fractures, and in the low altitude neck central area, by highly sheared blocks, forming ridges, alternating with chaotic crushed zones. b. Comparison with a classical fault zone or shear zone model, modified from[22], showing high similarity with 67P features, with increasing deformation grade toward its centre.

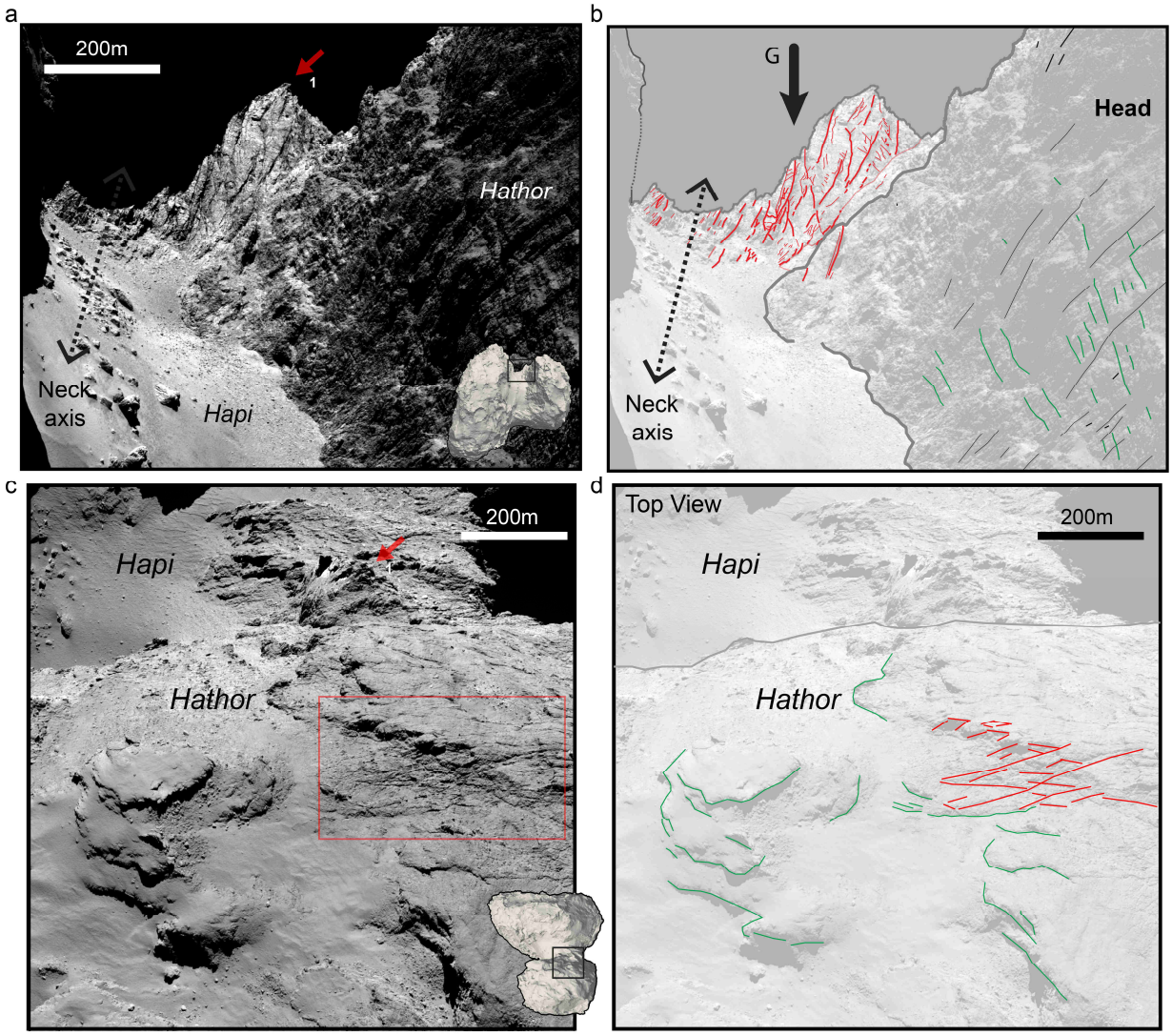

Supplementary Figure 7: Fracture pattern on Bakhu mount and NH equatorial region. a. Crop of NAC_2014-09-22T08.52.08.332Z_ID30_1397549001_F41 image showing mount-like topography (Bakhu) close to the neck centre. b. Fracture pattern (in red) showing two interconnected sub-vertical structures with opposite dip angles. Inferred layers on the Hathor cliff are in green, and clearly follow the topography contour lines. c. NAC_2016-06-16T09.32.11.500Z_ID30_1397549300_F22 image showing a top view of the same area (arrow indicating mount summit on both images.), where 3D observations of individual layers has been possible. d. Digitalised layer terraces (in green) and fracture pattern (in red) characterised by a typical multiscale diamond-shaped Riedel-shear structure (cf. Fig.S8), similar to that observed in SH.

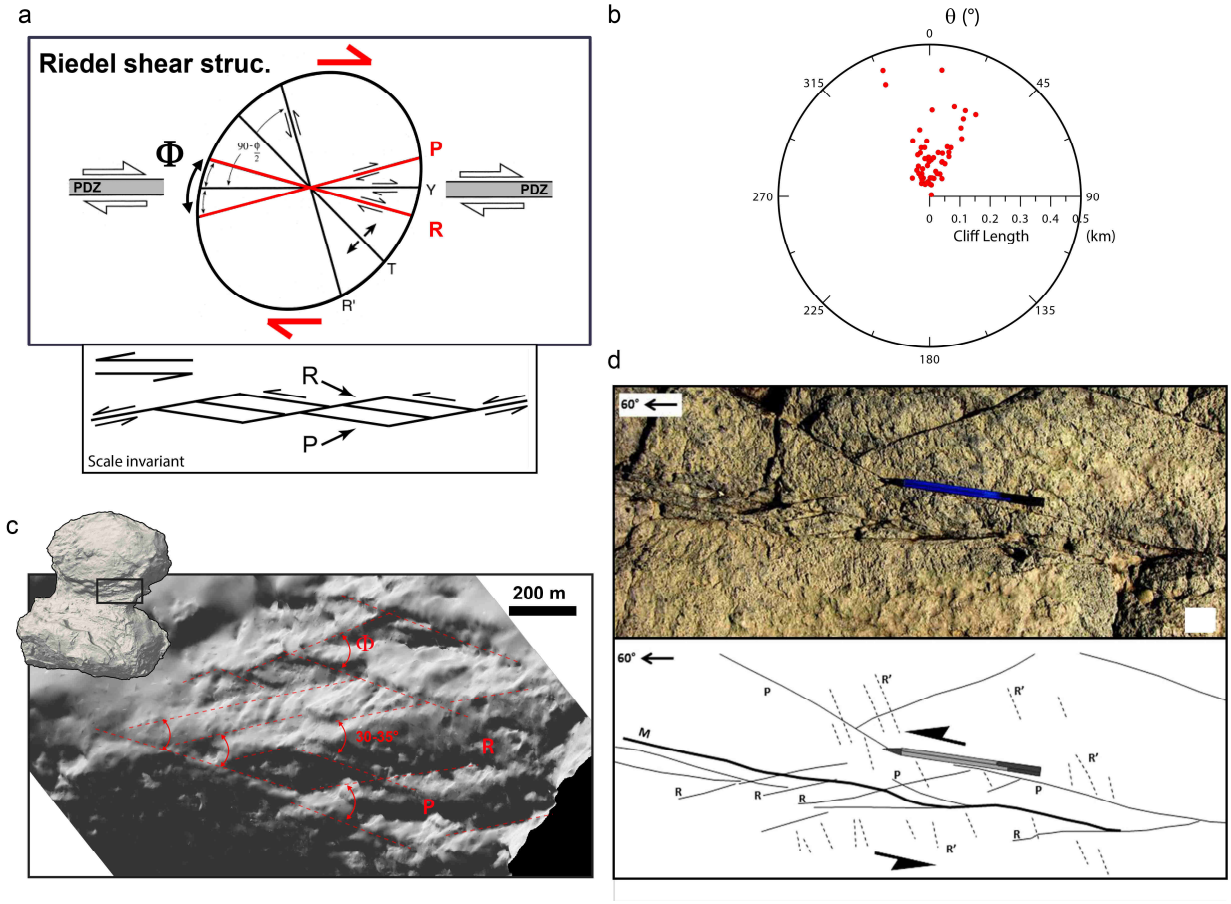

Supplementary Figure 8: Illustration of the Riedel-shear structure and its occurrence on 67P. a. Riedel-shear diagram showing fracture directions existing at all scales in a sheared material. P and R planes (in red) are dominant in 67P, forming a characteristic diamond shape pattern (lower box) which can be observed at all scales and is scale invariant (modified from [28]). Angle Φ between P and S Riedel-shear fractures corresponds to the internal friction angle of the material (modified from[53]), which matches with previously estimated angle on 67P. b. Polar plot of the cliffs directions, measured on the neck borders, directly on the 3D shape model (see methods) and showing similar separation angle than the fractures. c. Cliffs and ridges direction (in the Neck's centre) on the 3D shape model forming an angle around 30° and diamond-shape patterns, highly similar to a Riedel-shear pattern. d. Earth example of a decimetre scale Riedel-shear pattern showing essentially R and P planes (from[48]). This pattern shows striking similarity with pattern observed on fractures-related cliffs and ridges on the 3D shape model.

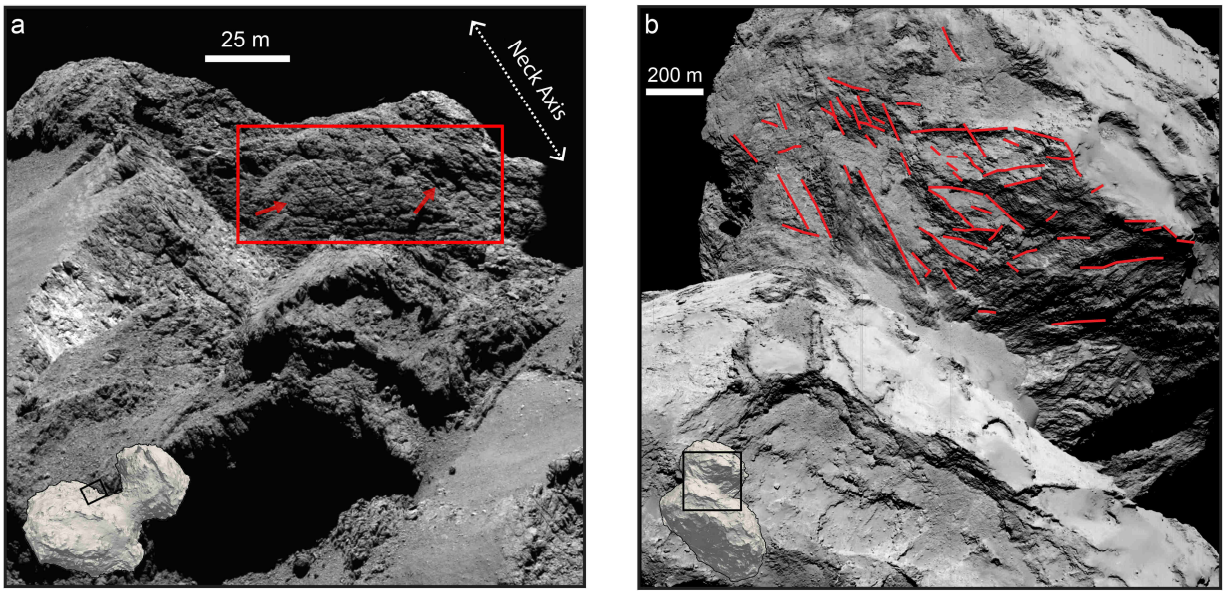

Supplementary Figure 9: Fracture pattern and cliff directions in NH regions. a. Crop of NAC_2016-08-06T07.23.48.276Z_ID30_1397549001_F22 image of the Hapi cliffs showing (in red boxes) 2-direction fracture patterns (arrows), similar to those observed in the SH. b. Image NAC_2015-02-22T10.28.00.838Z_ID30_1397549001_F24 of Hathor cliff exhibiting two marked cliff directions (underlined in red), and suggesting a similar pattern (as observed in the SH) for the fractures that formed these cliff after the erosion/collapse of one side of the fracture plane.

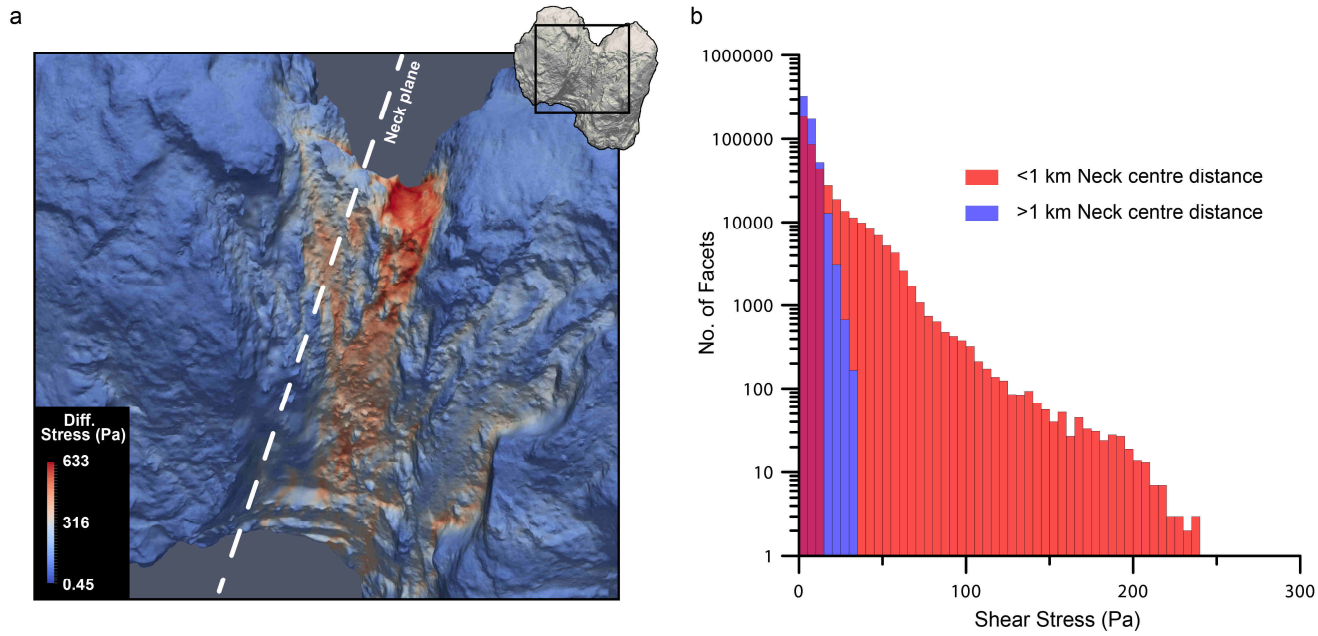

Supplementary Figure 10: Stress model in the neck area of 67P's nucleus. a. Differential stress magnitude (in Pa) mapped on the nucleus shape model surface, showing maximum differential stress concentrated in the Neck centre, where the highest deformation features have been observed. b. Shear-stress magnitude in the direction perpendicular to the neck axis (i.e. the direction of the shear deformation features observed) at >1 km distance from the neck centre (in blue) and < 1 km distance (in red), where it shows values higher than 100 Pa (i.e. the previously estimated shear strength of the nucleus material).

References:

46 Kim, Y.-S., Peacock, D. C. P. & Sanderson, D. J. Fault damage zones. Journal of Structural Geology 26, 503-517, doi:10.1016/j.jsg.2003.08.002 (2004).

47 Lee, J. a. R. C. M. a. C. A. Quaternary faulting history along the Deep Springs fault, California. GSA Bulletin 113, 855, doi:10.1130/0016-7606(2001)113<0855:QFHATD>2.0.CO;2 (2001).

48 Faulkner, D. R. & Rutter, E. H. Can the maintenance of overpressured fluids in large strike-slip fault zones explain their apparent weakness? Geology 29, 503 (2001).

49 Misra, A. A., Bhattacharya, G., Mukherjee, S. & Bose, N. Near N–S paleo-extension in the western Deccan region, India: Does it link strike-slip tectonics with India–Seychelles rifting? International Journal of Earth Sciences 103, 1645-1680, doi:10.1007/s00531-014-1021-x (2014).

50 Petit, J. P., Proust, F. & Tapponnier, P. Criteres de sens de mouvement sur les miroirs de failles en roches non calcaires. Bulletin de la Societe Geologique de France S7-XXV, 589-608, doi:10.2113/gssgfbull.S7-XXV.4.589 (1983).

51 Willingshofer, E., Sokoutis, D. & Burg, J. P. Lithospheric-scale analogue modelling of collision zones with a pre-existing weak zone. Deformation Mechanisms, Rheology and Tectonics: from Minerals to the Lithosphere 243, 277-294, doi:10.1144/gsl.sp.2005.243.01.18 (2005).

52 R.M., G., amp & Gunes Yilmaz, N. A new methodology for the analysis of the relationship between rock brittleness index and drag pick cutting efficiency. Journal of the Southern African Institute of Mining and Metallurgy 105, 727-733 (2005).

53 Davis, G. H., Bump, A. P., Garcia, P. E. & Ahlgren, S. G. Conjugate Riedel deformation band shear zones. Journal of Structural Geology 22, 169-190, doi:10.1016/s0191-8141(99)00140-6 (2000).